KINETICS OF ELECTRON TRANSFER AT SEMICONDUCTOR–ELECTROLYTE INTERFACES*

A. FUJISHIMA and S. NAKABAYASHI

Department of Synthetic Chemistry, Faculty of Engineering, University of Tokyo, Hongo, Bunkyo-ku 113 (Japan)

Summary

Highly exothermic electron transfer rates were measured using semiconductor electrochemical techniques. Experiments demonstrate that the decrease in the electron transfer rates with the exothermicity of the reactions in so-called abnormal regions is much more moderate than predicted classically, and this effect is probably due to intramolecular vibrations. On the basis of these results, we present a new kinetic model for interfacial charge transfer processes. Some preliminary results for the hole transfer rate are included.

1. Introduction

During the last decade there have been many attempts to develop photoelectrochemical solar energy transducers. As a result of these studies the efficiencies and/or the applications of photoelectrochemical reactions have been increased. However, we believe that there remain many undefined factors governing reactions at semiconductor–electrolyte interfaces.

One of the most important features of photoelectrochemical reactions occurring on large band gap semiconductor electrode surfaces is that the change in the free energy of the reaction is more negative than the reorganization energy of the redox species in the solution. The kinetics of the highly exothermic charge transfer reactions still requires clarification although progress in the theory of charge transfer kinetics in condensed phases has been made by Marcus [1], Levich [2] and Jortner and coworkers [3]. Impressive experimental results have been obtained by Rehm and Weller [4] and Beitz and Miller [5]. These show that in the highly exothermic region, where the changes in the free energy of the reactions are more negative than the reorganization energy, the electron transfer rates do not always obey classical predictions.

*Paper presented at the Fifth International Conference on Photochemical Conversion and Storage of Solar Energy, Osaka, Japan, August 26 - 31, 1984.

0047-2670/85/$3.30

The subject of this paper is divided into two parts. The first part is concerned with the measurement of the rate of electron injection from the conduction band to the electron acceptors in the solution [6 - 8]. Previous experiments have been performed under homogeneous conditions [4, 5]. The changes in the free energy of the reactions were controlled by the selection of appropriate donor and acceptor pairs. However, in our case, because of the heterogeneous nature of the system, it was possible to change the free energy of the electron transfer reactions continuously by changing the electrode potential. Therefore this semiconductor electrochemical approach enables the electron transfer rate profile to be evaluated as a function of the change in free energy. The second part of the paper is concerned with the measurement of the rate of hole transfer from the valence band to ferrocene, the hole acceptor in the solution [9]. The results of these experiments can be explained by the non-classical charge transfer model.

2. Experimental details

The measurements were divided into two parts:

(i) The rate of electron injection from the conduction band to the electron acceptors in the solution was measured. The electron acceptors used were (a) 9,10-diphenylanthracene (DPA), (b) the monocation radical of DPA ($DPA^{\ddagger}$), (c) the monocation radical of thianthrene ($Th^{\ddagger}$), (d) the monocation radical of deuterium-substituted thianthrene ($Th^{\ddagger}$-d_8) and (e) the ferricinium ion (Fc^{+}). These measurements were performed in the dark.

(ii) The hole transfer rate from the valence band to ferrocene, the hole acceptor in the solution, was measured under laser excitation.

Figure 1 shows the experimental arrangement. The cell for the electrolysis was totally isolated from the ambient atmosphere. The samples were prepared using a vacuum line. The solvent used was commercial spectrograde acetonitrile (ACN) which was dried over P_4O_{10}. The supporting electrolyte was tetrabutylammonium perchlorate (TBAP) which was recrystallized three times from ethanol–acetone mixtures. Deuterium-substituted thianthrene (Th-d_8) was prepared by recommended synthetic routes, and the other chemicals were obtained from commercial sources. The purities of these chemicals were checked by the usual cyclic voltammetric analysis using a platinum electrode. If necessary, these chemicals were purified by recrystallization from the appropriate solvents followed by sublimation. The cation radicals were produced by pre-electrolysis using a platinum electrode and were found to be stable with lifetimes of over 1 h under our experimental conditions. All electrochemical experiments were conducted in oxygen and water-free ACN–TBAP electrolyte.

The electrode system consisted of (1) a ZnO single-crystal electrode with a surface area in the range 10^{-3} - 10^{-2} cm^2 (kindly donated by Professor G. Heiland, F.R.G.), (2) a platinum electrode for pre-electrolysis, which was used for the production of the cation radicals, (3) a silver quasi-reference

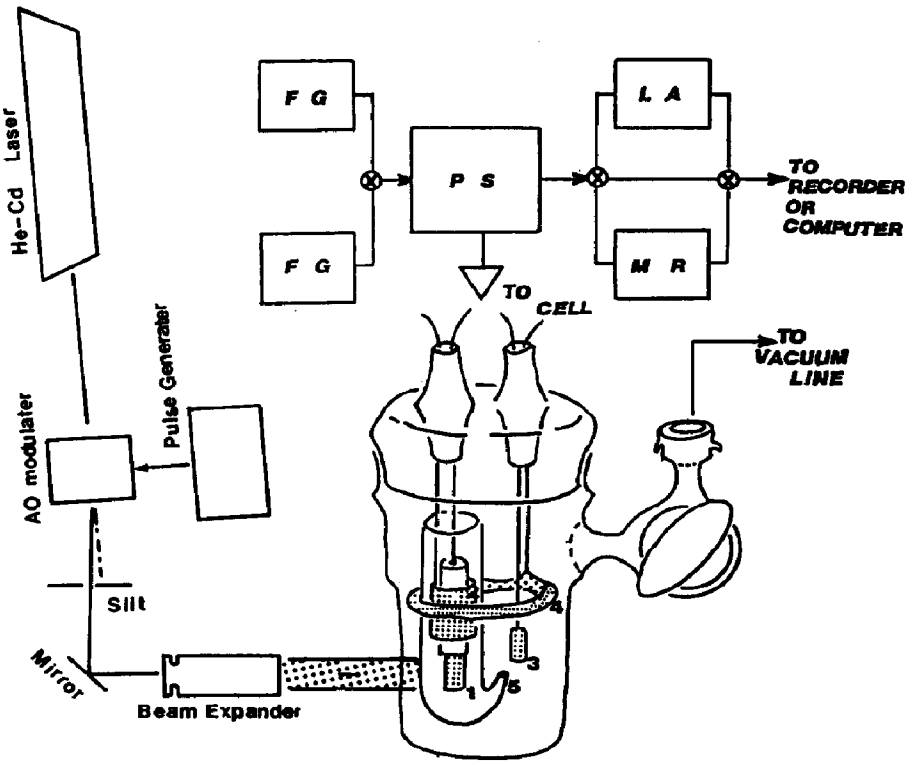

Fig. 1. Schematic diagram of the experimental arrangements: AO, acousto-optic; FG, function generator; LA, lock-in amplifier; MR, digital memory; PS, potentiostat.

electrode, (4) a platinum counterelectrode and (5) a separator (glass capillary). The pretreatment of the ZnO electrode followed the recommended procedure [10]. The appropriate set of electrodes, depending on the experiments, was selected from these five components.

To estimate the electron transfer rate for experiment (i), potential step chronoammetry was employed in a time domain of about 1 ms. The time-dependent current responses to the perturbation of the potential step were measured using a Toho Giken type 7070 high speed potentiostat, which has a reliable time domain of up to 100 μs for the load condition involved, and recorded using a transient memory (Kawasaki Electronica KR-3250 8 bits, 4 kwords). Electron transfer rates were extracted from these results by a curve-fitting procedure using theoretical equations.

In experiment (ii) the hole transfer rate was measured using two independent experimental procedures. In these experiments a conventional three-electrode cell was employed. In the first experiment the ZnO electrode was excited by continuous irradiation from an He–Cd laser. When the laser excitation was switched off sufficiently quickly (through an acousto-optic modulator capable of supplying the laser step with a time constant faster than 1 μs), a decrease in the transient photocurrent was observed and was recorded using the transient memory. In the second experiment

the illumination from the laser radiation was modulated by the acousto-optic modulator with modulation frequencies in the range 10 Hz - 20 kHz. The in-phase and out-of-phase components of the photocurrent response to this irradiation modulation were measured using an autophase lock-in amplifier (LI-575 NF circuit block).

3. Results and discussion

3.1. The rate of electron injection from the conduction band to the electron acceptors in the solution

In this experiment a ZnO electrode was used as the electron source, and DPA and the monocation and/or the monocation radicals in the solution were electron acceptors. All electron acceptors used are known to be outer-sphere electron transfer reagents. Energetically, the reaction for producing the anion radical of DPA (type I) is in the normal electron transfer region, while other reactions (type II) are in the abnormal region, as described later.

The changes in the reaction energy are discussed in this section. The flat-band potential for the ZnO single-crystal electrode in contact with the ACN–TBAP electrolyte under our conditions was found to be −0.3 V (Ag) (measured against a silver electrode) [6]. The formation of an accumulation layer was observed in the potential range −0.2 to −0.5 V (Ag) where most of the drop in the electrode potential occurred in the accumulation layer of the ZnO electrode. However, in the region $E < -0.5$ V (Ag) the electrode potential was found to drop in the Helmholtz layer in the liquid phase. This result confirms that changing the electrode potential in this region ($E < -0.5$ V (Ag)) makes it possible to vary the change in the free energy of the electron transfer reaction from the conduction band of ZnO to the electron acceptor in the liquid phase. The heterogeneous electron transfer rate from the conduction band of ZnO to the electron acceptor in the liquid phase was confirmed to be a linear function of an overlap of the electron density of states of the electron acceptor in the liquid phase provided that the adiabatic parameter of the reaction is independent of the electrode potential [11]. In this experiment the adiabatic parameter of the reaction is assumed to be constant for each redox species because the free-energy change is controlled by the electrode potential for a single redox species. The electron transfer rate is then governed by the line shape of the density of states of the electron acceptor in the liquid phase, a subject which will be dealt with in greater detail later.

Potential step chronoammetry was employed to estimate the electron transfer rate. The time-dependent current profile was found to obey the following equations for reactions of type I and type II respectively [6]:

$$i(t) = \frac{\Delta V}{R} \exp\left(-\frac{t}{RC}\right) + nFAk_c Co^b \left\{1 - \frac{2(k_c + k_a)t}{D}\right\} \qquad (I)$$

$$i(t) = \frac{\Delta V}{R}\exp\left(-\frac{t}{RC}\right) + nFAk_c Co^b\left(1 - \frac{2k_c t}{D}\right) \qquad \text{(II)}$$

In these equations the first term is non-faradaic and the second term is the linear-approximated faradaic term for the reversible (type I) and irreversible (type II) electron transfer processes. In reactions of type (I) the electron exchange occurs in the conduction band of the electrode, whereas in reactions of type (II) an anodic electron flow to the ZnO electrode is totally blocked by the forbidden region of the electrode. ΔV, R and C are the potential step height, the resistance and the capacitance of the cell respectively, k_c and k_a are the cathodic and anodic electron transfer rates respectively, Co^b is the bulk concentration and D is the diffusion coefficient of the electron acceptors. The other symbols have their usual meanings. Electron transfer rates at various potentials were extracted from the observed current–time curves, by curve-fitting procedures using the model equations given above.

The relationship between the electron transfer rate to DPA (reactions of type (I)) and the electrode potential is shown in Fig. 2. It can be seen that as the electrode potential becomes more cathodic (*i.e.* as the change in the free energy of the reaction becomes more negative), the electron transfer rate increases exponentially. The observed standard redox potential of DPA|DPA$^-$ at the platinum electrode was −1.7 V (Ag), whereas the value at the ZnO electrode was −1.8 V (Ag). The formal rate constant at the ZnO electrode was found to be about a tenth of that on platinum, probably because of the non-adiabatic character of the former reaction. The exponential increase in the electron transfer rate shown in Fig. 2 is the kinetic profile of the normal electron transfer reaction occurring at the ZnO electrode.

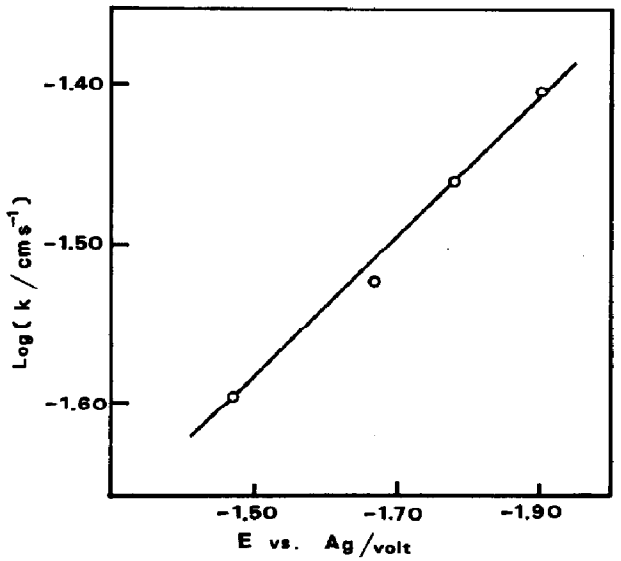

Fig. 2. Plot of the logarithm of the rate constant for the reduction of DPA on the ZnO electrode *vs.* the electrode potential.

Figures 3 - 5 show the kinetic profiles of the abnormal electron transfer reaction occurring at the ZnO electrode. Figure 3 shows the observed relationships between the rates of electron transfer to $DPA^{\dagger}$ and $Th^{\dagger}$ and the electrode potentials. The decrease in the rate with the exothermicity of the reaction, where the exothermicity increases with cathodic polarization, was found to be about 30% for a change in the electrode potential from −0.5 to −1.5 V (Ag), where the change in the free energy of the reaction is assumed to be from −1.75 to −2.75 eV with a deviation of about 0.2 eV. This

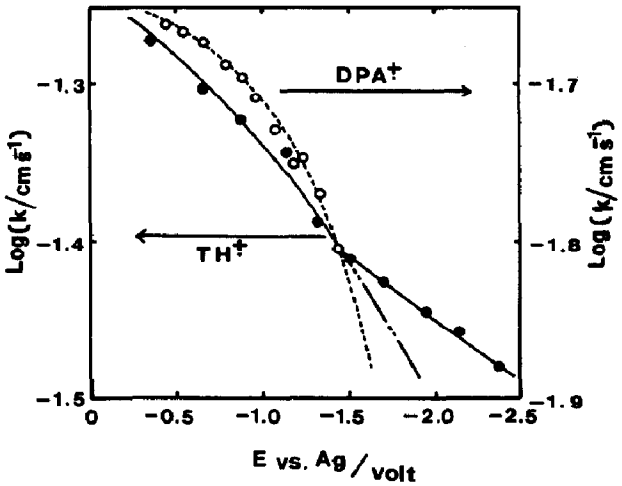

Fig. 3. Plots of the logarithm of the rate constant for the reduction of $Th^{\dagger}$ (●) and $DPA^{\dagger}$ (○) on a ZnO electrode *vs.* the electrode potential.

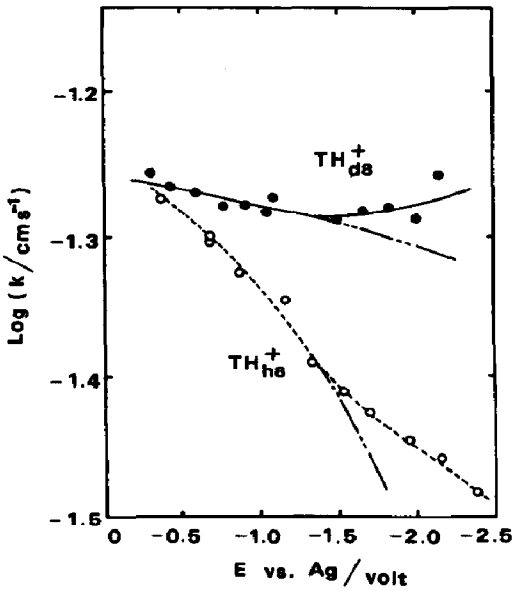

Fig. 4. Plots of the logarithm of the rate constant for the reduction of $Th^{\dagger}$ (○) and $Th^{\dagger}$-d_8 (●) on a ZnO electrode *vs.* the electrode potential.

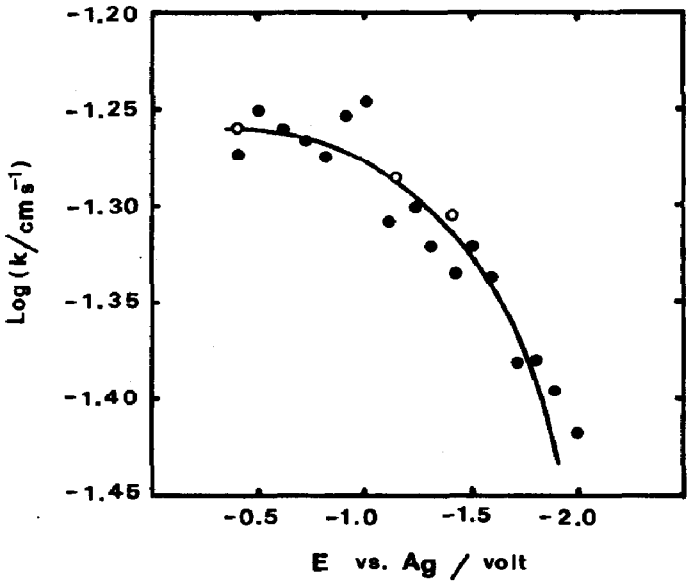

Fig. 5. Plot of the logarithm of the rate constant for the reduction of Fc^+ on a ZnO electrode *vs.* the electrode potential.

deviation is attributed to the energetic width of the electron accumulation layer at the electrode. These two redox couples (DPA|DPA^+ and Th|Th^+) have the same redox potential and their solvent reorganization energies are assumed to be similar. The rate decrease profiles of the two couples are almost the same at potentials which are more anodic than −1.5 V (Ag). Figure 4 shows the relationships observed between the rate of electron transfer to Th^+ and Th^+-d_8 and the electrode potentials. The redox potentials of Th|Th^+ and Th-d_8|Th^+-d_8 were found to be the same, *i.e.* +1.25 V (Ag). The rate decrease observed for the deuterium-substituted case was moderate. Figure 5 shows the relationship between the electron transfer to Fc^+ and the electrode potentials. The redox potential of Fc|Fc^+ was found to be +0.6 V (Ag). Therefore a change in electrode potential from −0.5 to −1.5 V (Ag) corresponds to a change from −1.1 to −2.1 eV with a deviation of about 0.2 eV. The smallest change in the free energy was observed for reactions of type II. However, the change in free energy from −1.1 to −2.1 eV is certainly more exothermic than its reorganization energy (approximately 0.5 - 0.6 eV), *i.e.* the electron transfer reactions described above are considered to be in the abnormal region.

The rate decreases observed for reactions of type II are a few orders of magnitude smaller than that predicted by the classical theory. However, the results show qualitative agreement with the experimental data of Rehm and Weller [4]. This discrepancy between the observations and the classical predictions suggests that the electron transfer rates in the abnormal region are incompatible with the fundamental postulate of classical theories, *i.e.* that the electron transfer rates depend solely on the solvent reorganization energy which is represented by the dielectric properties of the solvent and

the molecular volume of the reactant [1]. As previously pointed out by Jortner and coworkers [3], Levich [2] and other researchers [12], the intramolecular vibrational effects of the reactants must be considered in abnormal electron transfer reactions; it is expected that the decrease in the electron transfer rate in the abnormal region will be moderated by the vibrationally excited products. This situation will be explained below.

Figure 6 is a one-dimensional representation of the reaction coordinate for an electron transfer reaction and of course is a schematic representation of many real dimensions. Figure 6(a) shows that the change in the free energy of the reaction is more positive than $-\lambda$, where λ is the reorganization energy, clearly demonstrating the activation characteristic of this reaction. This situation corresponds to a reaction of type I. When the change in free energy becomes more negative than that shown in Fig. 6(a) such that $\Delta G = -\lambda$, electron transfer is expected to proceed by an activationless process (Fig. 6(b)). The electron transfer process reaches its maximum rate under these conditions. A further increase in the negativity of the free energy change, *i.e.* the character of the reaction becomes more exothermic, results in the reappearance of the activation energy (Fig. 6(c), full curve). Under these conditions the rate of the reaction is expected to decrease as the exothermicity of the reaction decreases. This situation is predicted by classical theory. However, if vibrational excitation of the product state is considered, the activation energy should be much lower than the classical value. These conditions are shown by the broken curves in Fig. 6(c) which explain the type II reactions. Thus, unless some unknown surface factors such as the surface states have an effect on the rate, the rate decreases shown in Figs. 3 - 5 reflect the vibrational excitation of the electron transfer products.

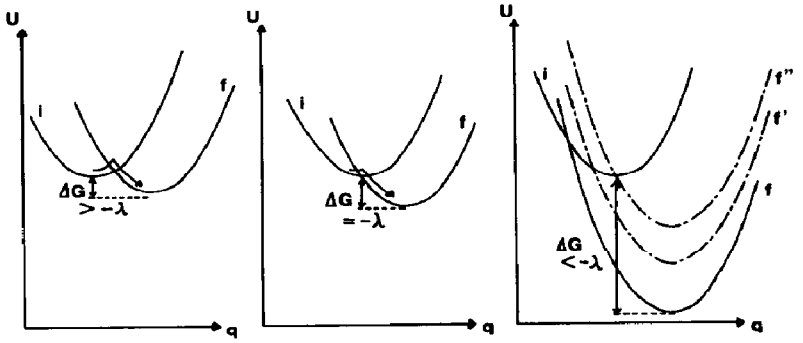

Fig. 6. Schematic representation of the potential surface for initial (i) and final (f) states: (a) the change ΔG in the free energy of the electron transfer reaction is greater than $-\lambda$, where λ is the reorganization energy ($\Delta G^{\ddagger} > 0$); (b) $\Delta G = -\lambda$ ($\Delta G^{\ddagger} = 0$); (c) ΔG is negatively greater than $-\lambda$ ($\Delta G^{\ddagger}$ depends on the vibration states) (——, vibrational excitation of the final state is not allowed; — · —, vibrational excitation of the final state is allowed).

3.2. The rate of hole transfer from the valence band to ferrocene in the solution

The rate of hole transfer was measured using two independent experiments, and the results were found to be in substantial agreement. The hole transfer occurred approximately as a pseudo-first-order process with respect to the hole concentration under our excitation conditions. The rate was found to be independent of the electrode potentials.

Ferrocene is known to undergo simple outer-sphere one-electron oxidation in an aprotic medium such as ACN. The concentration of ferrocene in the electrolyte was 10^{-2} M. Before performing the kinetic experiments, the overall reaction profiles of this photoelectrochemical reaction were measured using the rotating ring–disc electrode (RRDE) technique; a polycrystalline ZnO disc electrode was used and the ring electrode was a conventional platinum electrode. These experiments showed that the photocurrent was dominated by ferrocene oxidation; 90% of the photocurrent was due to the oxidation of ferrocene and the rest was probably due to photocorrosion of the ZnO electrode. The disc photocurrents were found to be independent of the rate of rotation of the electrode which means that the photocurrent was limited by the concentration of photoexcited holes in the electrode.

The results of the first experiment are shown in Fig. 7. After the continuous laser excitation was switched off a transient photocurrent profile was recorded at each electrode potential. These transient photocurrents $I(t)$ were normalized using the continuous value $I(0)$ for each

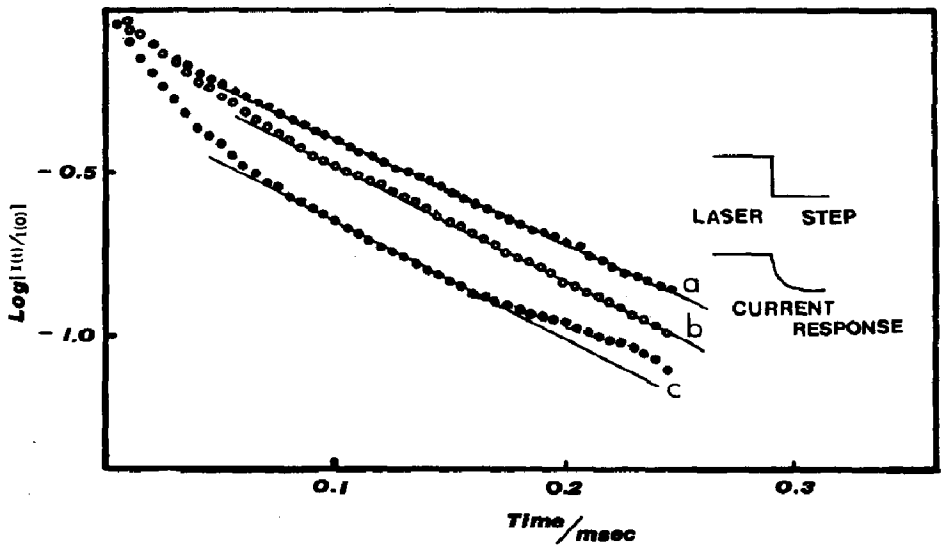

Fig. 7. Plot of the logarithm of the normalized photocurrent $I(t)/I(0)$ *vs.* time at various electrode potentials ($I(0)$ is the continuous photocurrent of the ZnO electrode excited by an He–Cd laser; $I(t)$ is the time-dependent photocurrent transient observed when the laser irradiation is switched off sufficiently quickly): curve a, 0.5 V (Ag); curve b, 0.85 V (Ag); curve c, 1.4 V (Ag).

electrode potential, and the logarithms of the transient photocurrents were plotted against time. This time region ($t > 0.1$ ms) is reliable since the time constant of the cell, which was deduced from measurements of the cell impedance, was much less than 0.1 ms. Further, the slopes observed in Fig. 7 were found to depend on the photoelectrochemical reactions. For example, the transient current in the absence of a reducing reagent, where the decomposition of the electrode is predominant, was totally different from that in the presence of a reducing reagent. Therefore the slopes in Fig. 7 are assumed to represent the first-order kinetics of the hole transfer from the electrode to the ferrocene. The rate was found to be about 10^4 s^{-1}, independent of the potential.

The results of the second experiment are shown in Fig. 8. The laser radiation was modulated by an acousto-optic modulator at frequencies of 10 Hz - 20 kHz. The in-phase and out-of-phase components of the photocurrent response to this irradiation modulation were measured and plotted for each electrode potential. Each curve in Fig. 8 shows one grand arc in the frequency region from 100 Hz to 20 kHz and quite complicated behaviour in the lower frequencies. In the former frequency regions the relaxation functions of the photocurrent are approximated by a Debye-type function, which is in substantial agreement with the result of the laser step experiment described above. Then it is possible to deduce the time constant from the frequency of the minimum of the grand arc as follows: $\tau = 1/2\pi f$ where f is the frequency of the minimum of the arc and $1/\tau$ is the first-order rate constant of the hole transfer. From Fig. 8, f was found to be about 1.5 kHz and independent of the potential. The rates were then calculated to be about 10^4 s^{-1}, independent of the potential.

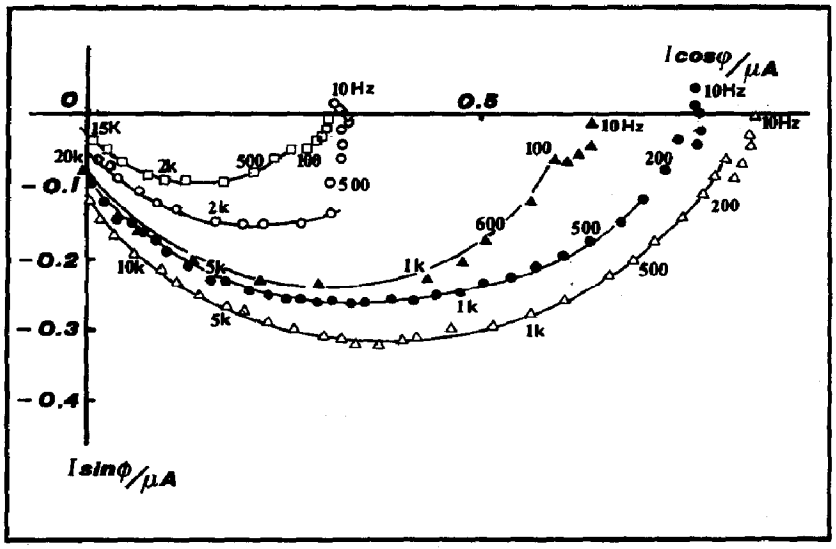

Fig. 8. The in-phase and out-of-phase photocurrents $I \cos\varphi$ and $I \sin\varphi$ as functions of the irradiation modulation frequencies at various electrode potentials: □, 0.5 V (Ag); ○, 0.75 V (Ag); ▲, 1.0 V (Ag); ●, 1.25 V (Ag); △, 1.5 V (Ag).

Our results show that the rates of hole transfer to ferrocene are independent of the electrode potential and suggest that the direct hole transfer may occur from the top of the valence band to ferrocene in the solution. However, the change in the reaction energy of this process is approximately −2.3 eV, which is more negative than the reorganization energy. Therefore the direct hole transfer mechanism is not allowed in the context of the classical predictions.

4. Conclusion

The results of the first experiment lead to the conclusion that intramolecular vibrations, such as C—H vibrations, play a decisive role in electron transfer kinetics in the abnormal region. To include these effects the classical theory illustrated in Fig. 9(a) must be corrected as shown in Fig.

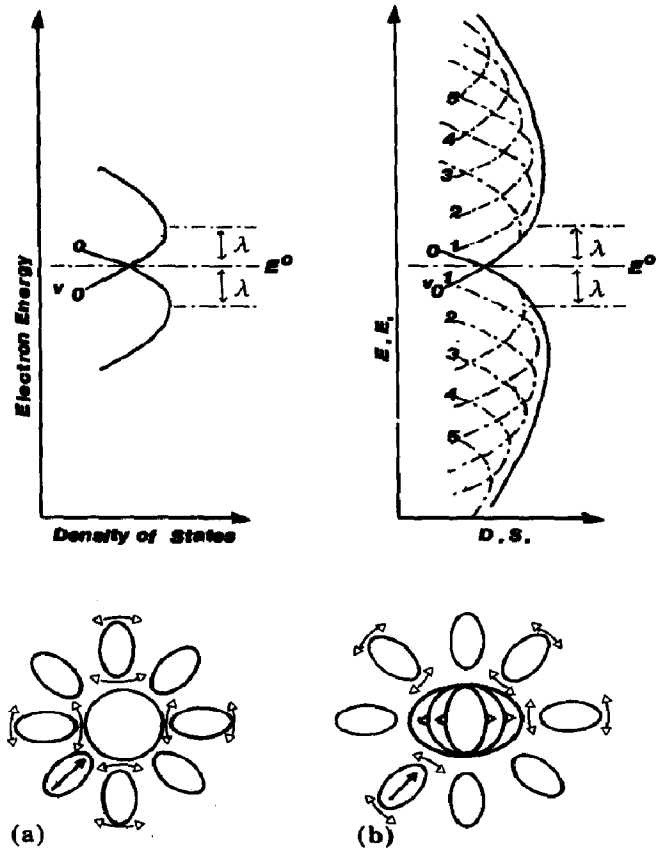

(a) (b)

Fig. 9. Schematic representation of the correlation between (a) the classical model and (b) the vibronic model (upper full curves, acceptor line shape function; lower full curves, donor line shape function): — · — (parabolae), line shape functions for each molecular vibrational state v; ——, thermally averaged summation of each parabola (*i.e.* each molecular vibrational state).

9(b) to account for slow decreases in the rate in the abnormal region because of the intramolecular vibration-assisted line shape function of the density of states in the liquid phase. This intramolecular vibration-assisted line shape function allows for direct hole transfer from the top of the valence band to the reducing agent. Our preliminary results for the rate of hole transfer to ferrocene obtained in the second experiment support this interpretation.

These results were used to derive the schematic representation of the mechanism of the heterogeneous charge transfer reactions shown in Fig. 10. The figure shows that (a) one possible mechanism for the hole transfer reaction is the surface-state-assisted process and (b) another mechanism is the vibrational-assisted process. Process (b) is quite important in the case of non-Fermi-level pinning materials for which the surface state density at the electrode is low [13].

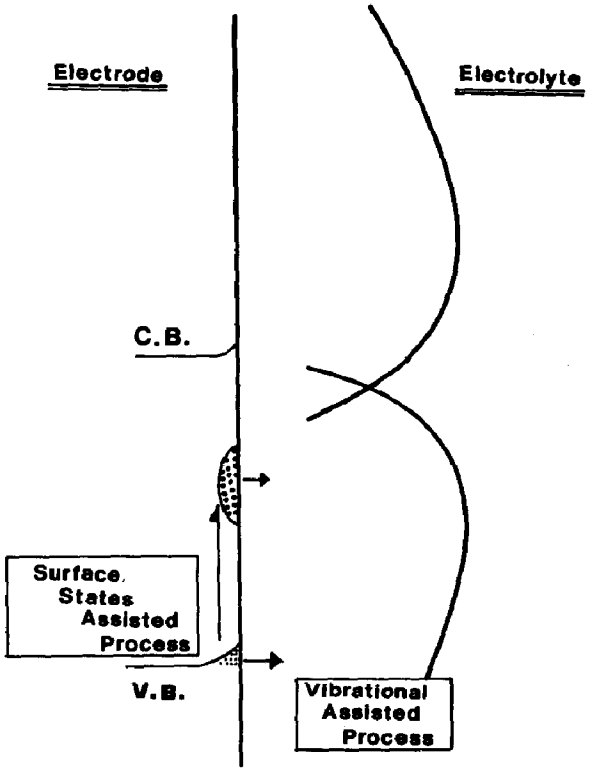

Fig. 10. Schematic representation of the hole transfer mechanism occurring at the large band gap n-type semiconductor electrode.

References

1 R. A. Marcus, *J. Chem. Phys.*, *24* (1956) 966, 979; *26* (1957) 867, 872.
2 V. G. Levich, *Adv. Electrochem. Electrochem. Eng.*, *4* (1966) 249 - 372.

3 J. Jortner, *J. Chem. Phys.*, *64* (1975) 4860.
J. Ulstrup and J. Jortner, *J. Chem. Phys.*, *63* (1975) 4358.
J. Jortner, *J. Am. Chem. Soc.*, *102* (1980) 6676.
E. Buhks, M. Bixson and J. Jortner, *J. Phys. Chem.*, *85* (1981) 3763.
4 D. Rehm and A. Weller, *Ber. Bunsenges. Phys. Chem.*, *73* (1969) 834; *Isr. J. Chem.*, *8* (1970) 259.
5 J. V. Beitz and J. R. Miller, *J. Chem. Phys.*, *71* (1979) 4579.
6 S. Nakabayashi, A. Fujishima and K. Honda, *J. Electroanal. Chem.*, *140* (1982) 223.
7 S. Nakabayashi, A. Fujishima and K. Honda, *J. Phys. Chem.*, *87* (1983) 3487.
8 S. Nakabayashi, K. Itoh, A. Fujishima and K. Honda, *J. Phys. Chem.*, *87* (1983) 5301.
9 S. Nakabayashi, S. Miyabe, A. Fujishima and K. Honda, *J. Electroanal. Chem.*, *157* (1983) 135.
10 P. A. Kohl and A. J. Bard, *J. Am. Chem. Soc.*, *99* (1977) 7532.
W. P. Gomes, T. Freund and S. R. Morrison, *J. Electrochem. Soc.*, *115* (1968) 818.
11 H. Gerischer, *Adv. Electrochem. Electrochem. Eng.*, *1* (1961) 139 - 232.
12 J. Ulstrup, *Charge Transfer Processes in Condensed Media, Lecture Note in Chemistry 10*, Springer, Berlin, 1979, and references cited therein.
13 A. J. Bard, A. B. Bocarsly, F. F. Fan, E. G. Walton and M. S. Wrighton, *J. Am. Chem. Soc.*, *102* (1980) 3671.